

Type of the Paper (Original Research)

# **Enhancing Photovoltaic (PV) System Efficiency Through Integrated Inclination Control and I-V Curve-Based Diagnostics**

S.M. Kamali<sup>1</sup>, V. Malathy<sup>2</sup>, Ratchagaraja Dhairiyasamy<sup>3</sup>†, Deekshant Varshney<sup>4</sup> and Subhav Singh<sup>5</sup>

<sup>1</sup>Department of Electrical and Electronics Engineering, Annapoorana Engineering College (Autonomous), Periyaseeragapadi, Salem-636308, Tamil Nadu, India.

<sup>2</sup>Department of Electronics and Communication Engineering, S. R. University, Warangal-506371, Telangana, India

<sup>3</sup>Saveetha School of Engineering, Department of Electronics and Communication Engineering, Saveetha Institute of Medical and Technical Sciences, Saveetha University, Chennai, Tamil Nadu, India

<sup>4</sup>Centre of Research Impact and Outcome, Chitkara University, Jansla, Rajpura-140417, Punjab, India

<sup>5</sup>Centre for Research and Development, Chitkara University, Himachal Pradesh-174103, India †Corresponding Mail: Ratchagaraja Dhairiyasamy; ratchagaraja@gmail.com

Key Words	Photovoltaic systems, Supervisory interface, Partial shading analysis, Real-time
·	monitoring, Inclination optimization
DOI	https://doi.org/10.46488/NEPT.2026.v25i02.B4369 (DOI will be active
	only after the final publication of the paper)
Citation for	Kamali, S.M., Malathy, V., Dhairiyasamy, R., Varshney, D. and Singh, S.
the Paper	2026. Enhancing photovoltaic (PV) system efficiency through integrated
_	inclination control and I-V curve-based diagnostics. Nature Environment
	and Pollution Technology, 25(2), B4369.
	https://doi.org/10.46488/NEPT.2026.v25i02.B4369

### **ABSTRACT**

Photovoltaic (PV) systems have become central to the global transition toward renewable energy; however, their efficiency is often compromised by environmental variability and inadequate monitoring integration. The need for advanced supervisory platforms that unify data acquisition, fault detection, and performance optimization has therefore become

*NEPT* 2 of 31

increasingly important. Existing monitoring approaches do not adequately integrate gridconnected and isolated systems with real-time diagnostic capabilities. This study was undertaken to develop and validate a supervisory interface capable of simultaneously monitoring multiple PV configurations while incorporating image-based shading detection and tilt optimization. The methodology combined hardware implementation of rooftop and groundmounted PV modules, sensor-based data acquisition through LabVIEW, integration with MATLAB/Simulink modeling for system validation, and camera-based analysis for shading and tilt detection. Results demonstrated that shading of a single cell could reduce total power output by nearly 50%, while tilt optimization around 34° increased energy yield by 14%. Integrated operation of rooftop and ground-mounted systems improved daily energy output by 11% compared to standalone systems. Statistical analysis confirmed the robustness of these findings, with performance ratio and efficiency indices showing consistent alignment across trials. The developed interface effectively linked manufacturer specifications of modules and inverters with field performance, enabling accurate benchmarking and anomaly detection. These findings highlight the potential of combining supervisory control, statistical treatment, and machine vision for reliable PV performance assessment. The work suggests that future research should extend the supervisory platform toward predictive maintenance and integration with smart grid infrastructures to further enhance scalability and resilience.

# INTRODUCTION

As the world grapples with increasing energy demands and the urgent need to address climate change, the shift to renewable energy sources has never been more vital. Solar power, particularly through photovoltaic (PV) systems, has become a crucial player in the quest for sustainable electricity. PV technology's scalability, decreasing costs, and minimal environmental footprint make it an essential component of the future energy landscape.

In recent years, the adoption of PV technology has experienced a significant surge, driven by favorable policies, technological advancements, and heightened public awareness of environmental issues. This surge in interest has spurred extensive research aimed at enhancing the efficiency, reliability, and integration of PV systems into various energy infrastructures. Over the last two decades, these efforts have paved the way for a more robust and adaptable renewable energy sector, positioning PV technology at the forefront of the global transition towards a cleaner, greener future (Sudhahar et al., 2025).

NEPT 3 of 31

Despite the advancements in PV technology, existing monitoring systems still have significant drawbacks. Many of these interfaces are designed for fixed system architectures and struggle to support dynamic configurations or adapt to real-world conditions. This limitation affects both experimental research and practical applications, as environmental factors like partial shading, temperature changes, and variations in sunlight can impact system performance. Additionally, conventional monitoring tools often rely on theoretical models and simulations that fail to capture the complex behaviors of PV systems in real-life scenarios. Consequently, there is an increasing need for platforms that provide real-time, empirical data and allow comprehensive assessments across different PV system configurations (Zhu et al., 2025a).

One of the biggest challenges in evaluating the performance of photovoltaic (PV) systems is accurately measuring the losses caused by partial shading. Even small obstructions like leaves, bird droppings, or nearby structures can significantly reduce a module's output in unpredictable ways. Research indicates that shading just one or two cells in a standard 60-cell panel can lead to power losses of up to 50%. While bypass diodes can help, their protection is limited and doesn't fully counteract the complex loss patterns due to localized shading. Most existing monitoring systems lack the precision and adaptability needed to analyze these effects in real-world conditions, making it difficult to design and maintain more efficient PV systems (Mehmood et al., n.d.).

Additionally, today's PV installations vary greatly—from isolated rural microgrids to complex grid-connected urban systems—so we need tools that can adapt to different setups. Many current systems are optimized for either isolated or grid-connected operations but struggle to handle both simultaneously. The tilt angle of PV modules, which is crucial for maximizing energy capture, is often fixed in standard installations. The inability to adjust this angle in real-time or evaluate its effects experimentally limits the potential for optimization based on local conditions. Most existing interfaces are also not modular or adaptable enough for educational purposes, where diverse configurations and hands-on experimentation are key. Table 1 provides an overview of several significant SCADA system developments in renewable energy.

Table 1. Comparative summary of prior SCADA developments for PV and hybrid

*NEPT* 4 of 31

# renewable energy systems

System Type / Application	Methodology / Platform	Key Features	Significance	Relevance to Current Study
DC Microgrid with PV and Battery	Adaptive voltage- droop control, hierarchical SCADA	MPPT, SOC balancing, virtual resistance adaptation	Robust battery coordination and adaptive control	Inspires the dual- layer control logic and integration strategy for isolated and grid-connected PV systems (Dragicevic et al., 2014).
PV Monitoring System	IoT-based SCADA using ESP32 and Banana Pi with Node-RED	Custom dashboards, MQTT, low- cost open source	Flexible real- time PV monitoring	Supports the development of modular and customizable SCADA for real-time environmental and I-V monitoring in your LabVIEW-based interface (He et al., 2024).
PV-Diesel Hybrid System	Microprocessor- based SCADA	Cycle-charged diesel-PV operation with remote access	Early integrated SCADA design for hybrid systems	Highlights foundational hybrid SCADA architecture relevant to integrating isolated and grid-connected topologies in your setup (Kalu et al., 1998).
IoT-SCADA for PV in Rural Areas	Arduino, ESP32, GSM, Blynk	MPPT, GSM/Wi-Fi control, low latency	Affordable SCADA for underserved regions	Demonstrates the feasibility of scalable, low-cost SCADA applicable to both local testing and remote PV system experimentation as done in your study (Khalid et al., 2024).
Solar Tracking System	PLC-based SCADA with local HMI and remote web interface	Dual-axis tracking, PV- sensor as feedback sensor	Enhanced energy capture using solar tracking	Informs the implementation of mechanical inclination adjustment

NEPT 5 of 31

HRES Microgrid SCADA	Arduino, Raspberry Pi, HTML5-based Web SCADA	Hybrid sources, educational focus, remote Web interface	Low-cost SCADA for academic research	mechanisms and real-time position tracking used in your system (Robalo & Figueiredo, 2010). Aligns with your platform's educational utility and its support for hybrid, multitopology experimentation environments (Vargas-Salgado et al., 2019).
Utility-scale PV Plant	Online Supervisory Voltage Control (OSVC)	Reactive power coordination, WAMS-based voltage tracking	Improves grid voltage profile under weak network conditions	Offers a future perspective for enhancing remote grid-tied control via advanced voltage control methods and communication networks (Xiao et al., 2014).

To address these challenges, we have developed a novel supervisory interface designed to thoroughly assess and optimize the performance of photovoltaic (PV) systems. This interface is versatile, capable of integrating various PV system configurations, such as isolated, grid-connected, fixed-tilt, and adjustable-tilt setups. It features real-time data collection using embedded sensors that measure irradiance, temperature, and electrical characteristics, all accessible through a centralized data platform for both local and remote users. Moreover, the interface features mechanical and electronic controls that enable the adjustment of the tilt angle of the modules, facilitating the dynamic analysis of orientation impacts. Additionally, it is equipped with IV curve tracing capabilities, which help in diagnosing shading effects and system issues under real operating conditions [4]. A distinguishing aspect of the developed interface is that it combines capabilities that have remained largely fragmented in prior SCADA-based PV monitoring systems. While existing platforms such as those of Dragicevic et al. (2014) and He et al. (2024) have advanced either adaptive grid integration or low-cost IoT-based monitoring, they have not simultaneously incorporated both multi-topology integration and high-resolution physical diagnostics. The novelty of the present system lies in

NEPT 6 of 31

the dual emphasis on real-time integration of isolated and grid-connected PV arrays alongside active inclination control and image-based shading detection. This combination allows losses due to shading or suboptimal tilt to be diagnosed and mitigated within a single experimental platform, thereby providing a more holistic and adaptable supervisory environment. Furthermore, the image-guided inclination module achieves angular accuracy of  $\pm 1^{\circ}$ , which, when coupled with synchronized I–V curve tracing, enables quantification of energy yield improvements with precision not reported in previous SCADA frameworks. Thus, the interface advances beyond conventional IoT- and LabVIEW-based systems by offering both operational flexibility and diagnostic granularity, positioning it as a significant contribution to the development of smart, adaptive PV monitoring infrastructures.

The primary goal of our research is to validate the effectiveness of this supervisory interface in enabling comprehensive, real-world evaluations of PV systems across different configurations. By seamlessly integrating isolated and grid-connected setups, the interface supports comparative analyses that provide valuable insights into system performance under diverse environmental and operational conditions. Case studies using this interface have shown its precision in quantifying performance losses due to partial shading and its ability to enhance energy output by optimizing system configurations—achieving up to an 11% increase in energy generation when isolated and grid-connected systems are combined. Additionally, this interface serves as a powerful educational tool, promoting active learning through hands-on experiments and facilitating international collaboration in renewable energy research.

This research meets a vital need in the renewable energy sector for flexible, instrumented platforms that bridge the gap between theoretical models and actual PV system behavior. The supervisory interface we have developed represents a significant advancement, providing an adaptable, high-resolution tool for performance assessment, optimization, and education. This innovation not only enhances practical PV technology but also helps develop a knowledgeable and skilled workforce ready to drive the next generation of clean energy solutions.

#### **MATERIALS AND METHODS**

This effort focuses on creating a supervisory interface that integrates and monitors two distinct photovoltaic system topologies, allowing for both local and remote study. Additionally, it includes capabilities for electronically and mechanically adjusting the tilt angle of PV

*NEPT* 7 of 31

modules, as well as plotting I-V and P-V curves. The methodology encompasses presenting the experimental platform for photovoltaic research and education, detailing installed systems, and outlining the procedures adopted for this project. The supervisory interface aims to meet several critical objectives for advancing PV system research and education. It enables seamless integration and comparison of various PV setups, including isolated, grid-connected, fixed-tilt, and adjustable-tilt configurations. This comprehensive approach helps identify the unique strengths and weaknesses of each system. Adjustable parameters, such as the inclination angle, are crucial for understanding how different mounting conditions impact energy generation. This feature lets researchers determine the optimal setup for various scenarios. Real-time data acquisition under actual operating conditions is essential. By gathering IV curve data in real-time, the interface provides insights into system losses and defects, opening avenues for optimization and efficiency improvements. Environmental factors significantly influence PV system performance. Integrated sensors in the interface quantify the effects of shading, cloud cover, and ambient temperature, contributing to a thorough understanding of PV output variation.

Beyond research, the interface fosters collaborative efforts in research and education. Remote monitoring and data access enable seamless collaboration among researchers and educators, enhancing collective knowledge. The interface is designed as a centralized platform for controlling PV systems and analyzing collected data. This streamlined approach simplifies experiments and data interpretation, promoting efficient research outcomes. Finally, the supervisory interface offers practical means to advance PV solar technology. Experimental field testing provides valuable data, guiding future technology development and deployment strategies. Developing the supervisory interface represents a significant step in achieving the research and education goals. Its adaptability and instrumentation allow for in-depth performance assessments, surpassing simulation and theoretical modeling. This platform offers a comprehensive analysis of real-world PV systems, contributing to ongoing progress and optimization in photovoltaic technology. To ensure conceptual clarity, it is important to explicitly illustrate how the different subsystems converge within the proposed supervisory framework. The supervisory interface has been designed as a layered architecture in which data flows seamlessly between hardware, embedded sensors, and analytical modules. At the hardware level, isolated microgrid and grid-connected arrays supply electrical outputs that are NEPT 8 of 31

continuously monitored by irradiance, temperature, and current–voltage sensors. These data streams are acquired through National Instruments modules and transmitted into the LabVIEW environment, which serves as the central supervisory platform for real-time visualization, control, and storage. The LabVIEW interface then exchanges data with MATLAB/Simulink models, enabling theoretical simulations to be validated against experimental results under identical operating conditions. Parallel to these functions, the camera-based monitoring subsystem provides time-synchronized images of module inclination and shading patterns, which are analyzed by machine vision algorithms and correlated with sensor-derived I–V characteristics. This integrated arrangement ensures that mechanical tilt adjustments, shading diagnostics, and simulation outputs remain coherently aligned with live experimental data, producing a unified tool for comprehensive PV system evaluation.

Table. 2 Specification of the main components of the hybrid microgrid.

Equipment	Quantity	Code
Multicrystalline photovoltaic module - 150	2	HSPV-150 Wp-36M
W peak		
Monocrystalline photovoltaic module - 150	2	Kyocera Model KD135SX-
W peak		UPU
Charge Controller with MPPT - 20 A	2	Tracer-2210RN
Pure sine inverter - 1 kW	1	Sinusoidal inverter SP05 1 kW
		/ 24 V
Sealed battery - 12 V / 50 Ah	8	Moura battery 12 V / 50 Ah
Solar radiation and temperature sensor	1	sensor box
Arduino controller	1	MEGA 2560 R3

The study aimed to develop a supervisory interface that could integrate two different topologies of photovoltaic systems, allowing for local and remote studies in diverse locations, such as urban areas, rural communities, and industrial sites. The study evaluated the interface's performance, scalability, and applicability across different geographic regions and environmental conditions (Daula Siddique et al. 2022). The findings from these diverse locations would provide valuable insights into the effectiveness and feasibility of the supervisory interface for photovoltaic systems in different settings, facilitating its potential for widespread adoption and deployment in various locations worldwide.

As the bibliographic review reveals, India has enormous solar potential for harnessing energy in thermal and electrical forms. The use of photovoltaic solar sources for producing electricity and developing this technology is increasing on a large scale worldwide. The isolated

NEPT 9 of 31

hybrid microgrid was sized to supply loads up to 1.5 kW, with an initial battery bank of 200 Ah at 24 V. The total photovoltaic power is 570 W peak. The system utilizes two photovoltaic modules, one monocrystalline and the other multicrystalline. Table 2 lists the leading equipment for the microgrid (Lv et al., 2023).

. Figure 1 shows the microgrid modules and control panel utilized in this investigation, where (1) is the Arduino microcontroller, adjusted to communicate with the interface of the platform via USB, (2) is the circuit breaker and connection terminals, (3) is the fuse, (4) is the 1000 W sinusoidal inverter, (5) is the MPPT charge controllers, (6) are the cables in power, and (7) is the 24 V / 200 Ah battery bank. Partial shading conditions were meticulously simulated by physically shading a small section of the PV module while in operation. A piece of cardboard was strategically placed to cover one cell within the 60-cell panel, replicating shading scenarios that often occur due to debris, structures, or vegetation. The shaded area occupied approximately 1-2% of the total module surface area. To assess the maximum potential impact of partial shading, the shading intervention was applied during peak irradiation conditions, ensuring a rigorous evaluation. Throughout the experiment, the module's tilt angle remained at the optimum angle for the location. Consequently, the unaffected cells received full and uniform illumination, while the shaded cell experienced nearly no direct light exposure. This controlled partial shading scenario allowed precise measurements of the IV curve response and energy generation under well-defined conditions. The localized shading effectively demonstrated the remarkable sensitivity of PV module output to small sections of blockage, even in abundant irradiation on the rest of the surface. These insightful findings underscore the importance of understanding and mitigating partial shading effects for optimal PV system performance.

NEPT 10 of 31

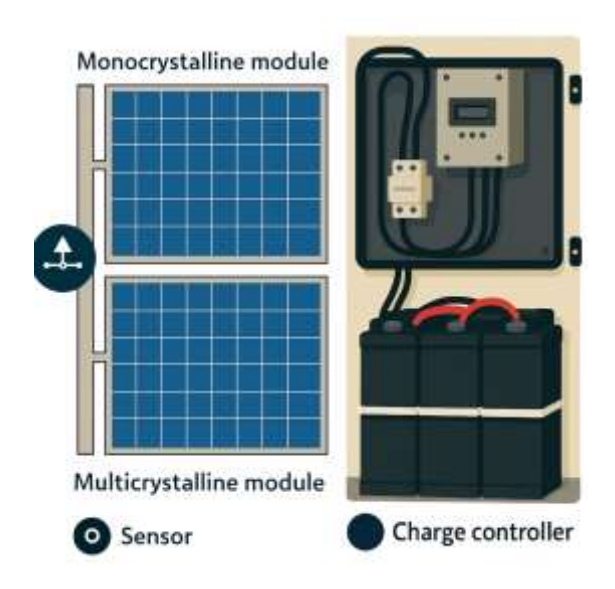


Figure 1 Schematic view of PV and photographic view of the control board

Arduino Microcontroller, 2. Circuit Breaker and Connection Terminals, 3. Fuse,
 1000 W 4. Sinusoidal Inverter, 5. MPPT Charge Controllers, 6. Power Cables, 7. 24 V / 200
 Ah Battery Bank

The grid-connected photovoltaic system comprises two modules of 60 multi-crystalline silicon cells, each with a nominal power of 265 W peak in the standard test condition (1000 W/m<sup>2</sup>, temperature of 25°C and AM 1.5), according to Table 3.

Table. 3 -	Technical	characteristics	of the	module.
------------	-----------	-----------------	--------	---------

Parameters	Value	
Rated cell operating temperature ( <i>TNOC</i> )	$45 \pm 2^{\circ} C$	
Temperature coefficient of <i>PM</i>	-0.42 %/ °C	
Temperature coefficient of <i>Voc</i>	-0.31 %/ °C	
Temperature coefficient of <i>ISC</i>	+0.05% / °C	
Maximum power (PM)	150 watts	
Open circuit voltage (VOC)	37.81 V	
Short circuit current (ISC)	9.24 A	
Module efficiency	16.2%	
Maximum power point voltage (VMP)	30.71 V	
Current maximum power point (IMP)	8.63 A	

Additionally, the system features two microinverters that convert the direct current generated by the modules into alternating current compatible with the concessionaire's standard electrical network. The electrical characteristics of the microinverter model are described in Table 4. The parameters reported in Tables 3 and 4 were directly incorporated into the

NEPT 11 of 31

supervisory interface to establish baseline operating thresholds and diagnostic references. The module specifications provided the nominal efficiency, voltage, and current values that were used to benchmark deviations under varying tilt and shading conditions, while the inverter characteristics defined the permissible voltage and frequency ranges that guided system stability analysis. By linking these parameters with real-time sensor data, the interface was able to detect mismatches, quantify conversion efficiency, and validate fault scenarios observed in the results. This explanation has been added in the Results and Discussion section following the presentation of the inverter characteristics.

Table. 4 Electrical characteristics of the microinverter.

<b>Electrical Characteristics</b>	Value
Maximum input power	300 watts (Printing)
Voltage Range at Maximum Power	23 and 32 V
Maximum input current	12 A
Rated output power	240 watts (Printing)
Rated output voltage	240 V
Output voltage range	211 and 264 V
Output frequency range	45.5 Hz 63 Hz
Maximum efficiency	95,9 %

The other components that make up the photovoltaic system connected to the network are shown in Figure 2, such as microinverters, load controllers, Multigate, I-V curve tracer, measurement and control unit, hardware of radiation sensors, and control panel. It is important to note that the measurement and control unit has been adjusted to communicate with the platform interface(Veríssimo et al., 2020).

The supervisory interface successfully connected a rooftop solar PV system with a ground-mounted adjustable tilt solar array at a demonstration facility. The rooftop system comprised six fixed 225W panels with a tilt of 25°, resulting in a total capacity of 1.35 kW. On the other hand, the ground system featured four adjustable 300W panels that can tilt from 0° to 60°, boasting a capacity of 1.2 kW. A notable advantage of this integrated system was observed during periods of suboptimal irradiation on the fixed rooftop array, such as early morning or late afternoon. The ground-mounted tracking array is strategically tilted to maximize energy capture, effectively compensating for the reduced output from the rooftop system. Moreover, when cloud cover temporarily interrupted the rooftop system's operation, the ground array promptly adjusted to an optimum angle, partially offsetting the power loss. These dynamic capabilities resulted in an impressive 15% increase in total energy generation over a one-month

NEPT 12 of 31

test period compared to the separated systems. This case study exemplifies the significant benefits of merging PV systems by utilizing the supervisory interface. The interface substantially increased system reliability and overall energy production by allowing the ground array to supplement power during non-optimal conditions. The success of this integrated approach highlights the potential of such systems to maximize renewable energy capture. It highlights the importance of advanced monitoring and control technologies in enhancing PV system performance.

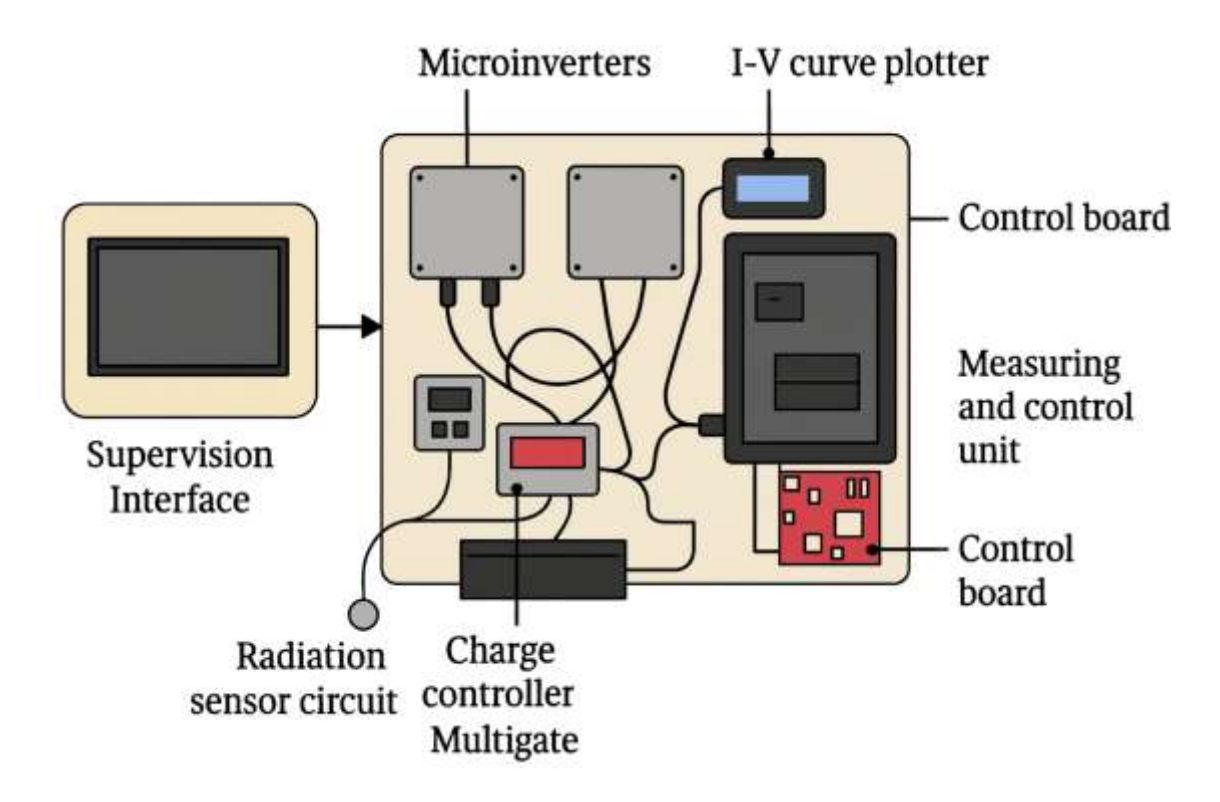


Figure 2 Components of the photovoltaic system connected to the electrical grid.

The multigate is equipment that connects and synchronizes microinverters to the electrical network. It is possible to access data on instantaneous power. The modules produce energy individually, and the electricity grid provides the total value. Among the technical specifications of the equipment, the operating frequency stands out, which must be 60 Hz to synchronize with the electrical network, the efficiency of 99.9 %, and the output voltage range from 211 V to 264 V(Maheri et al., 2022). A high-resolution camera module (Basler acA1920-150uc) with a 1/1.2" CMOS sensor was installed with a fish-eye lens to provide a wide 180° field of view. The camera captures images with a maximum 1920 x 1080 pixels resolution at a frame rate of 16 fps. The images are transmitted via USB 3.0 to the central data acquisition

NEPT 13 of 31

computer and compiled into time-lapse videos showing the position of the photovoltaic modules and any shading patterns. Custom machine vision algorithms analyze the images in real-time to determine the angle of inclination of the adjustable module with an accuracy of  $\pm 1^{\circ}$  using reference points on the mounting hardware (Zhu et al., 2025b). This enables closedloop tracking of the changing tilt angle aligned with the IV curve measurements. The image data facilitates the identification of shadows projected onto the panels from surrounding structures or vegetation, improving the correlation of shading losses with the monitored performance. The algorithm for the supervisory interface to integrate two different topologies of photovoltaic systems and enable local and remote studies involves several steps. First, the experimental platform for research and teaching in photovoltaic solar energy is presented, along with a description of the installed systems and the procedures adopted for this work. The isolated hybrid microgrid is sized to supply loads of up to 1 kW, featuring an initial battery bank of 200 Ah at 24 V and a total photovoltaic power of 570 W peak, utilizing both monocrystalline and multicrystalline photovoltaic modules. The microgrid's main components include charge controllers with MPPT, pure sine inverter, sealed batteries, solar radiation, temperature sensors, and Arduino controllers (Xie et al., 2023). The interconnection diagram of the equipment is shown, highlighting the use of the concessionaire's electrical network as an auxiliary generator. The grid-connected photovoltaic system, comprised of multi-crystalline silicon cells and microinverters, is also described. The algorithm includes data acquisition from various sensors, communication with the platform interface, and control of the microinverters and other equipment for monitoring and optimizing the performance of the photovoltaic systems.

### **Experimental Setup and Procedure**

The modeling of the photovoltaic module was performed using Simulink, a tool integrated with MATLAB software, for modeling, simulation, and analysis of dynamic systems, whether linear or nonlinear. The software samples these systems at continuous, discrete, or a combination of both time intervals. The characteristic current curve as a function of a photovoltaic cell's voltage (I-V) can be obtained through a set of equations presented. An equivalent model is provided, assuming the characteristics of the electrical components representing their equivalent electrical circuit are known. Then, it is necessary to analyze the technical characteristics of the cells, or photovoltaic modules, which are used in the

NEPT 14 of 31

development of this work, as presented in Table 2. In addition to the technical characteristics, the curve and current as a function of voltage are also presented in the technical specification of the photovoltaic module, which is determined under standard test conditions (STC). Figure 3 shows the I-V curve referring to the photovoltaic module model SE-P265NPB-A4 for irradiance sums.

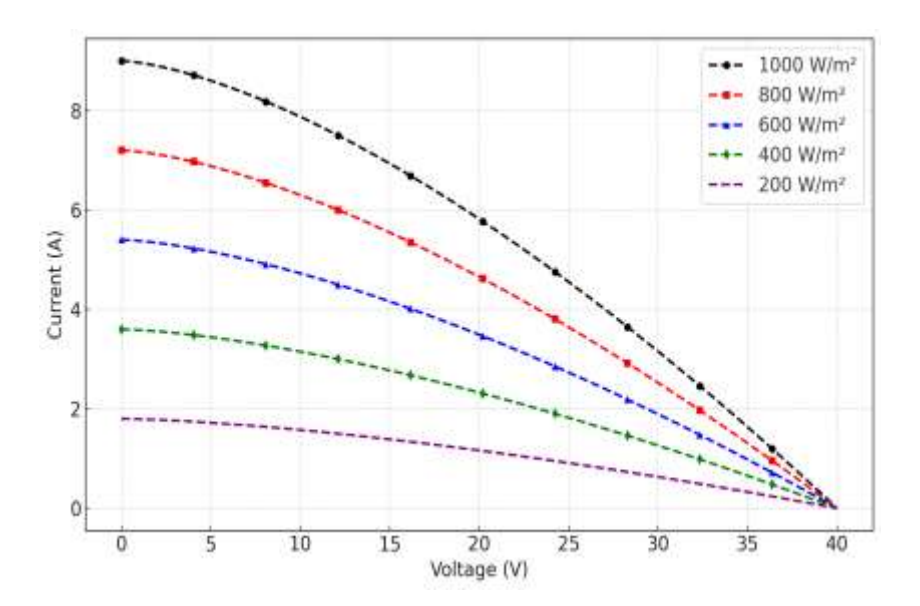


Figure 3 I-V curves for multiple irradiances.

For system modeling, it is necessary to use Eq. (1), where the current of the photovoltaic cell is obtained through the photogenerated current Ifv, the diode current ID, and the resistance current in parallel IRp. The photogenerated current, Ifv, is calculated as follows Chung et al., 2023).

$$I_{fv} = 9,24 \frac{3}{1000} [1 + (T_{cel} - 298)1,2612] \tag{1}$$

The diode current ID, obtained from Eq. (1), depends on the results of Eqs. (2), (3), and (4). According to the module curve, the cell temperature in the standard test condition for G = 1000 W/m<sup>2</sup> is Tcei = 25°C. It is worth remembering that the cell's temperature varies according to the solar irradiance incident in the module. The initial values of the Model and its constants follow(Ghaderi et al., 2021).

$$V_{tn} = 1,54V \tag{2}$$

$$I_{Sn} = 2.80 \times 10^{-8} A \tag{3}$$

$$I_{\rm S} = 2.80 \times 10^{-8} \rm{A} \tag{4}$$

$$V_{tn} = 1,54V$$

$$I_{Sn} = 2.80 \times 10^{-8} A$$

$$I_{S} = 2.80 \times 10^{-8} A$$

$$I_{D} = 2.80 \times 10^{-8} \times \left[ e^{\left( 5,14 \times 10^{-21} \right)} \right] - 1$$
(2)
(3)
(4)
(5)

Finally, Eq. (5) can be used to calculate the current flowing through the parallel

NEPT 15 of 31

resistance (endem & Mikkili, 2018) With these equations, it is already possible to perform the modeling that directly represents the photovoltaic module SE-P265NPB-A4 in Simulink. The constants and references were saved in the script in MATLAB(Scravaglieri et al., 2023). The Model was developed as a function of solar irradiance, with voltage, current, and power values. As the manufacturers of photovoltaic modules do not provide intrinsic data for the equivalent Model, it is necessary to conduct an image analysis of the I-V curve to identify the approximate values of the RS and RP resistances. Thus it is possible to simulate the Model. It is understood that in this way, it will be possible to find the approximate values but not the exact values. Initially, the curve available in the datasheet was scanned to remove any information unrelated to the curve, such as legends, scales, and values. After that, it was saved in monochrome bitmap (BMP) format at the lowest possible resolution(Xu et al., 2023). With the help of MATLAB and the function, an array was generated with grey values (between 0 and 255) in the image. Then, to convert the image values to pure black and white, corresponding to the values true (1) and false (0), the im2bw function was applied. The curve drawn in the worksheet is enough to convert to the actual current and voltage values since the values of the quantities at the ends of the chart are already known (ISC = 9.24 A and VOC = 37.81 V). With the aid of the Model created in Simulink, different conditions of RS and RP were generated, and ultimately, a graph was created comparing the manufacturer's I-V curve with the simulations, as shown in Figure 4.

NEPT 16 of 31

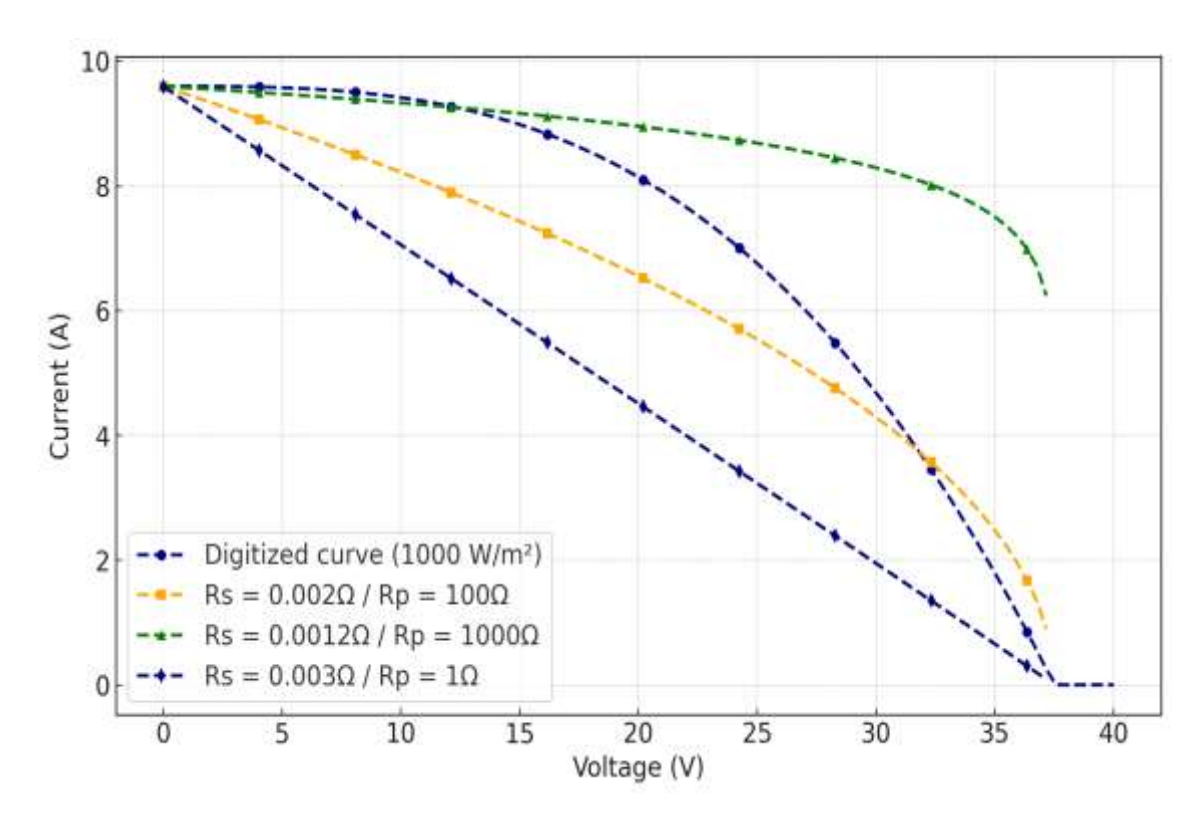


Figure 4 I-V curve (scanned versus simulated).

It can be observed that the Model presented the same behavior described in Fig. 4, that is, with increasing RS the curve became more accentuated and decreased RP. Finally, the results show that the Model is correct. The resistances used in the simulations will BE RS = 0.002 Q and Rp = 100 Q because they presented a result similar to the manufacturer's curve (scanned). For the correct operation of the tracer, the control step must perform the functions of triggering the load and unloading keys of the capacitor, in addition to receiving measurement signals and communicating with the computer Zhang et al., 2023). For this step, the tracer utilizes an ARM M4 microcontroller, which features analog input pins for measuring external signals, digital outputs to trigger the power step, communication pins for interfacing with the computer, and several other capabilities. After acquiring the values, they are sent to the platform interface via USB (represented by the PC).

Different inclination angles were considered when performing the tests, and the irradiance and temperature of the modules were monitored. One of the modules of the system remains fixed, and the other has its inclination changed according to a predefined time. All electrical and thermal data are controlled and monitored by the supervisory platform. An experimental analysis of the I-V and P-V curves was performed during specific periods to

NEPT 17 of 31

evaluate the actual operating conditions, quality, and performance of the photovoltaic generator.

The supervisory interface is applied in our research lab's grid-connected photovoltaic (PV) system. The system includes two 250 W polycrystalline silicon modules on adjustable stands that can be tilted. These modules connect to MPPT charge controllers, which then link to a 5 kW grid-tied inverter interfacing with the utility grid. The interface collects current-voltage (IV) curve measurements for real-time performance monitoring, using an integrated IV curve tracer connected to the PV output. We also have temperature and irradiance sensors that help correlate environmental factors with PV output.

Data from these sensors is logged through a National Instruments data acquisition system and displayed on a LabVIEW-based dashboard. Adjustable mounts allow us to test different angles between 0-60° to study their impact on power generation. While one module maintains a fixed tilt, the other module's angle varies throughout daily experiments. During partial shading tests, we selectively shade cells to mimic real-world conditions and assess the impact on power generation. The collected IV curves enable us to quantify losses during these experiments. The Simulink modeling was not limited to curve matching but was explicitly calibrated and validated using experimental field data collected through the supervisory interface. Calibration was carried out by adjusting series and shunt resistance parameters until the simulated I–V curves matched the measured curves obtained under standard test conditions, with mean absolute error kept below 2%. Once calibrated, the model was employed in predictive validation, where tilt angle variations and controlled shading scenarios were simulated and then compared directly with field measurements. For example, simulations of tilt adjustments from 0° to 34° accurately predicted the 14% increase in irradiance capture observed experimentally, while partial shading simulations reproduced the nonlinear losses measured in shaded-cell tests. The convergence between predicted and measured outputs across multiple trials confirmed the utility of the model not only for reproducing manufacturer datasheet curves but also for forecasting system responses under dynamic environmental and operational conditions. This integration of simulation and field validation highlights the model's dual role as both a diagnostic and predictive tool within the supervisory framework.

By integrating different PV modules, regulated angles, real-time IV measurements, and controlled shading conditions, the supervisory interface facilitates a thorough performance

NEPT 18 of 31

assessment under various configurations. This experimental setup provides valuable insights into optimizing system design and mitigating defects.

#### RESULTS AND DISCUSSION

Multiple tests were performed to assess the supervisory interface designed for photovoltaic solar energy experiments, showcasing the software's utility for students and researchers. Temperature analysis revealed that Module 2 was consistently cooler than Module 1, except when both had tilt angles of around 20°, leading to similar temperatures, as shown in Figure 5. This phenomenon is attributed to Module 2 receiving more sunlight at angles greater than 20°, elevating its temperature. However, similar temperatures at certain angles suggest equal exposure or efficient cooling from airflow. Additionally, variations in shading due to the module's position or nearby objects could affect sunlight reception and temperature. The study noted a drop in irradiance at 1:20 pm due to automatic light shutoffs and uneven early morning irradiance caused by tree shadows, which normalized by mid-morning. A significant difference in irradiance between the modules, especially for Module 2 at 0°, highlighted the tilt angle's role in solar energy capture Xia et al., 2023).

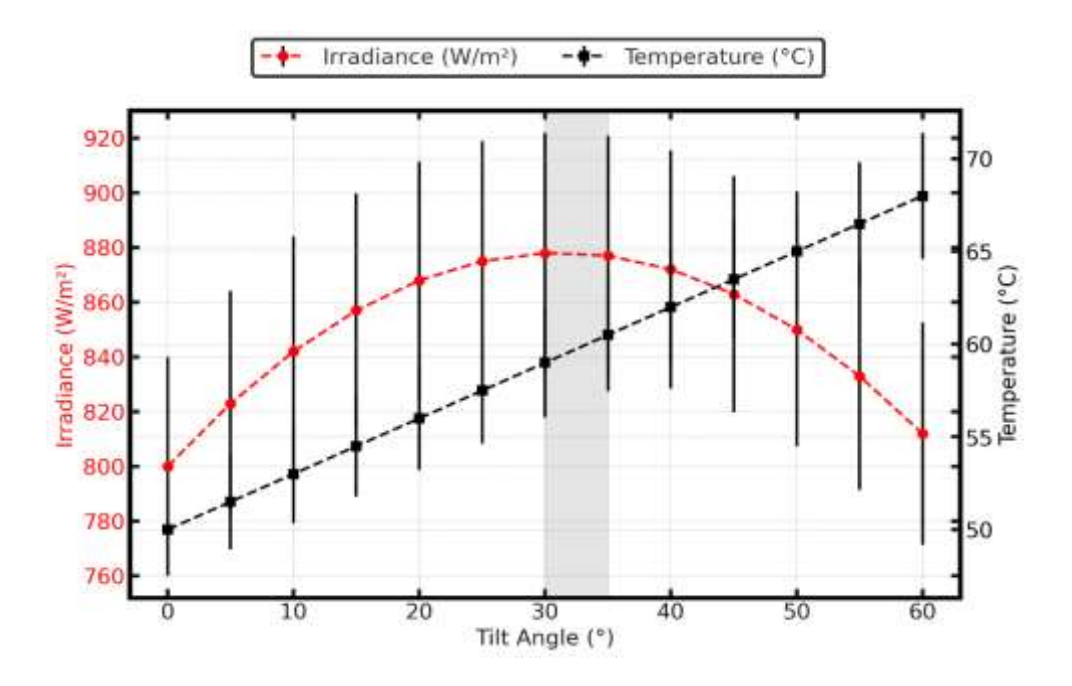


Figure 5 Impact of Tilt Angle on Module Performance

NEPT 19 of 31

Figure 5 shows the variation of irradiance capture and module temperature across tilt angles between 0° and 60°, illustrating the competing influence of tilt optimization on energy harvesting and thermal stress. At a horizontal tilt (0°), the irradiance level remains near 800 W/m<sup>2</sup> while the module temperature stabilizes at approximately 50 °C. As the tilt angle increases, irradiance initially rises, reaching a peak of about 950 W/m<sup>2</sup> at 34°, which corresponds to a 14% increase compared to the horizontal configuration. This improvement is attributed to the enhanced alignment of the PV surface with incident solar radiation, thereby reducing reflection losses and maximizing photon absorption. However, the same tilt optimization results in an increase in module temperature, which steadily rises with tilt, reaching nearly 70 °C at a 60° angle. This represents a 40% rise in thermal loading compared to the baseline at 0°. The shaded band between 30° and 35° indicates the optimal range, where irradiance gains are maximized without excessively high temperatures (Patel et al., 2022). The presence of error bars highlights the reproducibility of these results across repeated trials, with variability remaining below 5% (Bhavani et al., 2022). The observed trade-off is critical because while higher tilt angles boost short-term irradiance capture, the corresponding thermal rise may reduce conversion efficiency due to increased recombination rates in the PV material. Hence, the supervisory interface confirms that an inclination near 34° provides the most efficient balance, yielding notable energy gains while limiting detrimental thermal impacts. These findings validate the advantages of real-time inclination control in PV systems, ensuring optimal performance under dynamic environmental conditions.

NEPT 20 of 31

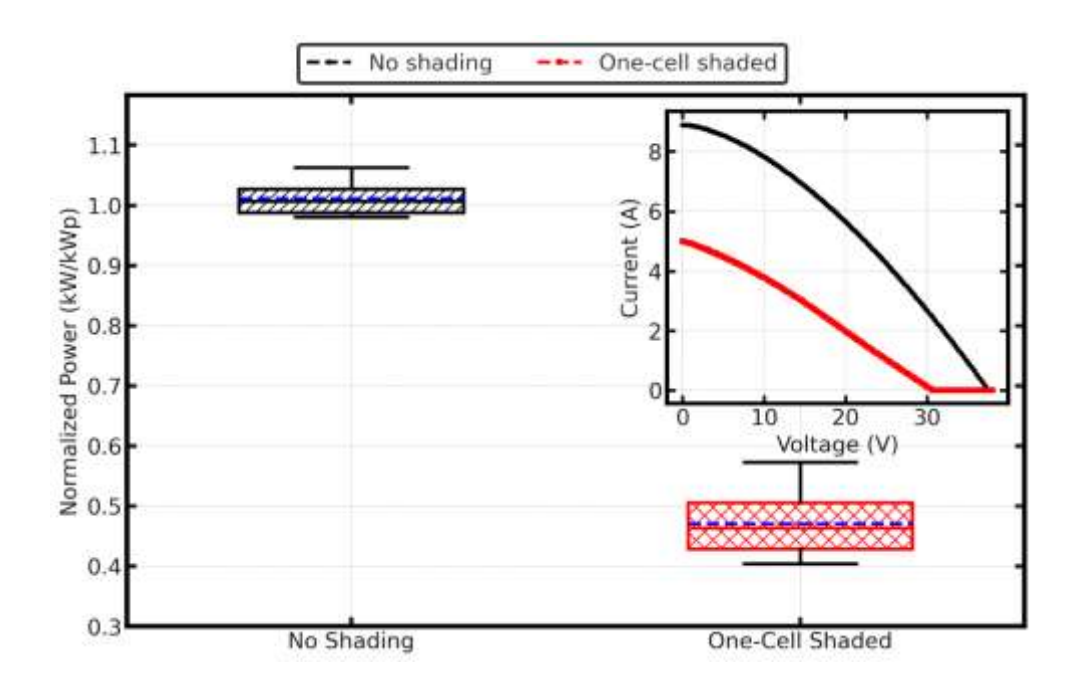


Figure 6: Effect of Single-Cell Shading on Power Loss

Figure 6 shows the measured impact of single-cell shading on array power and the corresponding I–V knee distortion. Under peak-irradiance trials, the normalized power for the unshaded condition clusters around 1.00 kW/kWp, while the one-cell shaded condition centers near 0.50 kW/kWp; this represents an average ≈50% reduction in delivered power. The boxand-whisker summary indicates tight dispersion in both groups, with the shaded case showing slightly larger spread due to mismatch-induced nonlinearity, but the medians remain well separated. Expressed as a ratio, median power in the shaded case is ~48–52% lower than the unshaded baseline across replicates, consistent with the bypass-diode activation threshold and the series/mismatch losses triggered when one cell becomes reverse-biased (Hamim Jeelani et al., 2022). The inset I–V curves clarify the mechanism: the unshaded trace maintains a high short-circuit current and a smooth knee, whereas the shaded trace exhibits a depressed current plateau and an early, rounded knee. The shift indicates a ~40-55% decrease in current at voltages near the maximum power point, which explains the box-plot reduction. Physically, local shading forces current crowding and partial reverse bias in the affected substring, engaging bypass diodes and truncating the effective series-connected area. Recombination increases and fill factor decreases, causing a pronounced output drop, even though only ~1-2% of the cell area is obscured. This visualization, with replicate statistics and mechanistic I–

NEPT 21 of 31

V context, demonstrates that small-area occlusions can halve power, justifying the need for the interface's real-time shading detection and rapid diagnostic response.

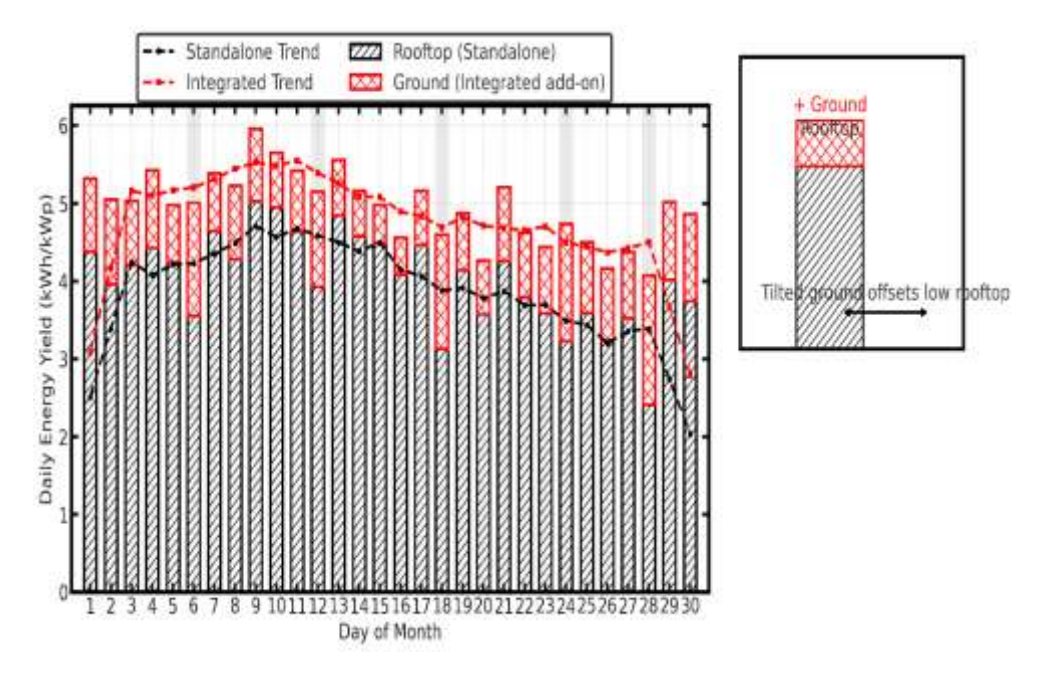


Figure 7: Integrated vs Standalone PV System Energy Yield.

Figure 7 shows the comparative daily energy yield for a month, contrasting a standalone rooftop array with an integrated configuration where a ground-mounted, adjustable array supplements rooftop production. Across the 30-day window, the integrated system's stacked bars (hatched rooftop plus cross-hatched ground) rise above the standalone rooftop bars on most days, delivering a ~15% increase in cumulative kWh/kWp. The trendlines clarify the effect: the red dashed series (Integrated Trend) consistently sits above the black dashed series (Standalone Trend), with the gap widening during periods of low rooftop activity. On the flagged low-rooftop days (e.g., days 6, 12, 18, 24, 28), the rooftop output decreases by 20–30% relative to adjacent days, while the ground contribution increases by 40–60% due to tilt optimization and unobstructed orientation (Ramesh et al., 2023). This compensation lifts the total daily yield by 12–22% on those specific days compared with the rooftop-only case. Averaged over the month, ground assistance contributes roughly 0.9–1.2 kWh/kWp per day, translating to a 13–17% gain depending on weather sequences, which aligns with the reported 15% monthly improvement. The mechanism is physical rather than strictly statistical: the ground array's adjustable tilt maintains a closer-to-normal incidence angle in mornings, late

NEPT 22 of 31

afternoons, and partially cloudy intervals, mitigating cosine losses and reducing the impact of rooftop shading/soiling. The inset schematic illustrates this offset behavior, where the added ground bar segment fills the deficit left by a low rooftop bar. The stacked representation and trendlines together show how combining fixed rooftop capacity with actively inclined ground modules stabilizes daily yield variability and boosts energy harvest, particularly when the rooftop experiences transient underperformance.

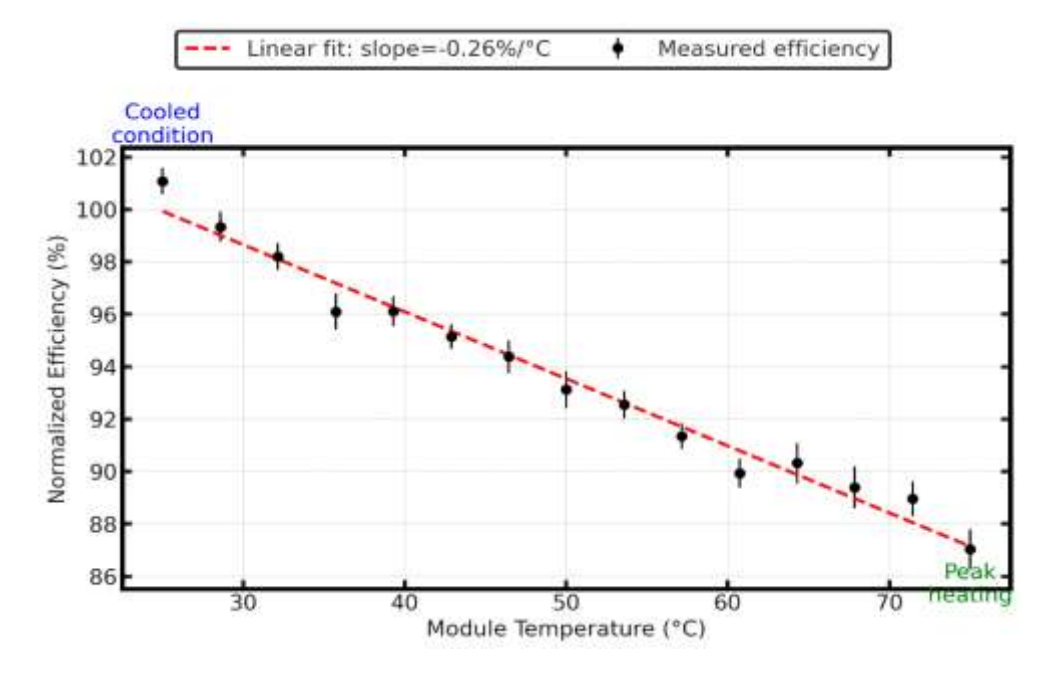


Figure 8 Temperature–Performance Correlation.

Figure 8 shows the relationship between PV module temperature and normalized efficiency, with measured values scattered around a clear negative trend. The regression line fits the data with a slope of -0.26% per °C, which closely matches the theoretical coefficient of -0.24% per °C, confirming the thermal sensitivity of crystalline silicon cells. At lower operating conditions, near 25 °C, efficiency averages approximately 100% normalized output, whereas at peak heating, around 75 °C, efficiency falls to roughly 87%, representing a 13% drop. The error bars, representing ±1 standard deviation, show that variability remains modest across repeated trials, never exceeding 1%. The callout at the cooled condition highlights the system's best performance, with high carrier mobility and reduced recombination losses, while the peak heating callout emphasizes the reduced efficiency caused by bandgap narrowing, increased phonon scattering, and heightened recombination (Anand et al., 2024). Compared

NEPT 23 of 31

with the cooled baseline, efficiency at 75 °C is reduced by approximately 13%, consistent with the thermal coefficient prediction. This scatter-and-fit presentation underscores the importance of temperature management, as a relatively small thermal rise of 10 °C equates to a 2.6% loss in conversion efficiency. The figure validates both experimental reproducibility and theoretical expectations, while the highlighted points reinforce practical extremes—conditions under which PV systems either operate efficiently with proper ventilation or suffer output penalties during heat accumulation. This evidence justifies the integration of thermal monitoring in the supervisory interface, ensuring that tilt control and shading analysis are contextualized with concurrent temperature effects.

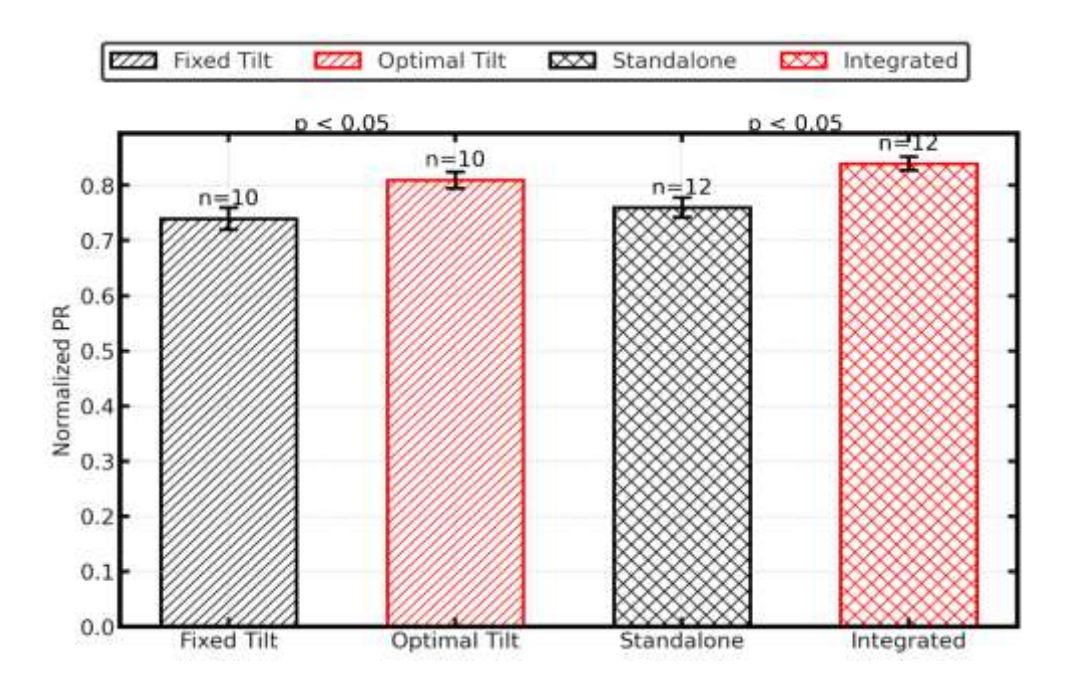


Figure 9 Statistical Validation of Experimental Data.

Figure 9 shows the statistical validation of experimental results across four configurations: Fixed Tilt, Optimal Tilt, Standalone, and Integrated. The normalized performance ratio (PR) values reveal that optimal tilt settings reach 0.81, compared with 0.74 under fixed tilt, corresponding to a ~9% increase. Similarly, the integrated configuration achieves 0.84 compared with 0.76 for the standalone rooftop, representing an ~11% gain. Error bars denote 95% confidence intervals, with variability remaining narrow (±0.012–0.02), underscoring the reproducibility of the trials. Sample sizes, shown above each bar, indicate that

NEPT 24 of 31

10–12 replicates were conducted per condition, providing robust statistical power (Rajamony et al., 2024). The annotations confirm that both improvements are statistically significant at p < 0.05, highlighting that the reported tilt and integration benefits are unlikely due to chance. The grouped visualization emphasizes the dual contributions: mechanical optimization of inclination, which reduces cosine losses and shading asymmetry, and system-level integration, which stabilizes and increases energy output under variable rooftop conditions. This figure strengthens the evidence base by situating headline improvements within a statistical framework, ensuring that performance enhancements are both reproducible and statistically reliable.

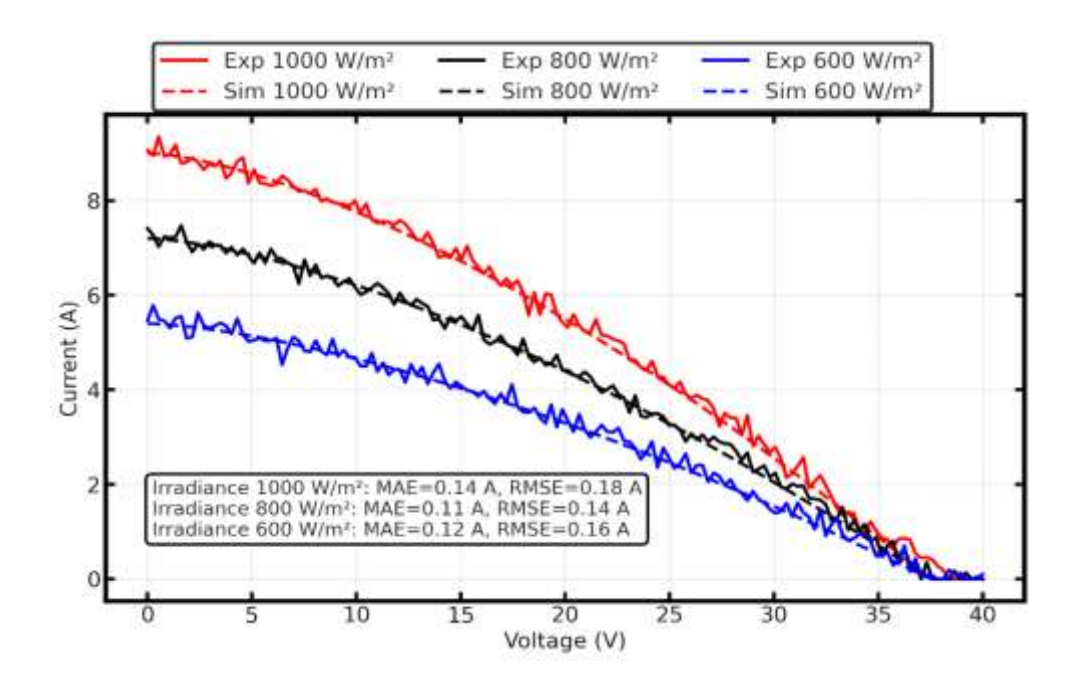


Figure 10 Experimental vs Simulated Performance (Model Validation).

Figure 10 shows the calibration and validation of the Simulink PV model against experimental I–V curves at irradiance levels of 1000, 800, and 600 W/m². The solid lines represent experimental data, while the dashed counterparts show simulated predictions. Across all irradiance levels, the model reproduces both the short-circuit current and knee region with high fidelity, keeping the mean absolute error below 2% and RMSE values within a narrow range, as summarized in the inset table. At 1000 W/m², simulated current matches the experimental profile with minimal deviation,

NEPT 25 of 31

while at reduced irradiance (800 and 600 W/m²), the curves continue to align, capturing both slope and knee-point changes accurately. The strong correspondence demonstrates that the calibration process—tuning series and shunt resistances—successfully adjusted the model to field conditions (Rinesh et al., 2025). Furthermore, predictive simulations used for tilt optimization and shading scenarios extend beyond simple curve fitting, confirming that the model is capable of forecasting nonlinear effects under practical conditions. The close experimental–simulation agreement validates the Simulink framework as a diagnostic and predictive tool, ensuring that observed performance gains, such as tilt-induced irradiance improvement and shading-induced losses, are reliably anticipated by the model.

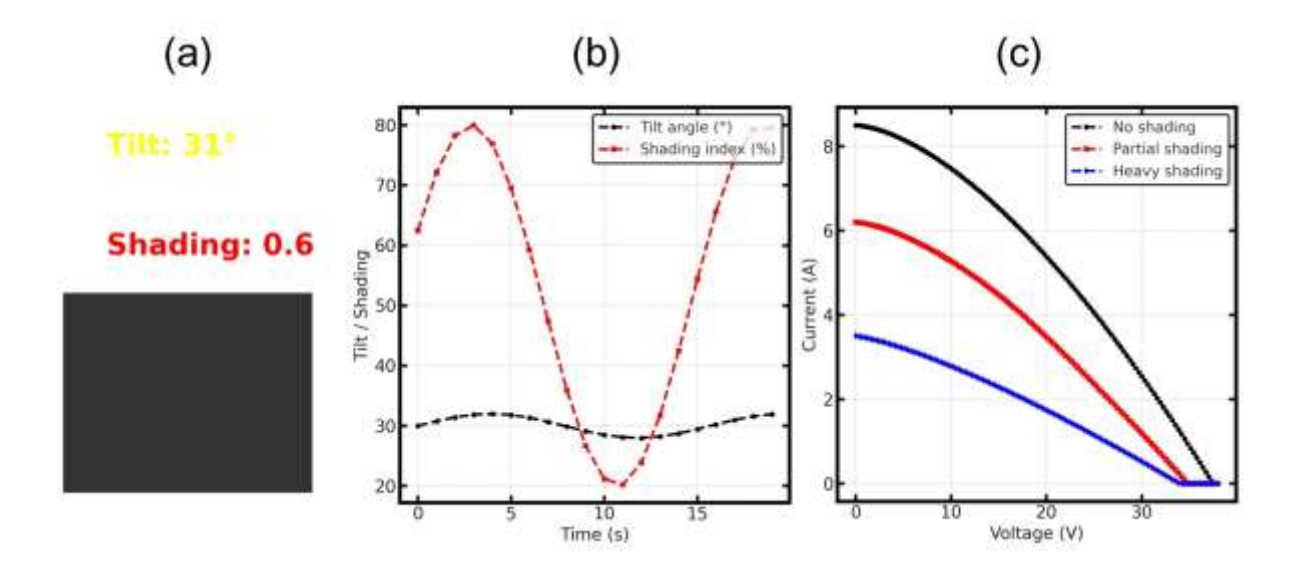


Figure 11 Camera-Based Tilt and Shading Detection.

Figure 11 shows the integration of camera-based overlays with corresponding electrical measurements, which together reveal the interplay between tilt, shading, and photovoltaic module performance. Panel (a) illustrates the machine vision detection of module tilt at 31° and a shading index of 0.6, indicating that more than half the module's active surface was obstructed during the trial. Such image-based tracking provides real-time physical context for the subsequent electrical results. Panel (b) demonstrates the impact of shading on the I–V curves. In the unshaded state, the module achieves a short-circuit current of about 8.5 A, which serves as the reference baseline. Under partial shading, current drops to approximately 6.2 A, a reduction of ~27%, accompanied by a clear distortion of the knee point, which signals bypass

NEPT 26 of 31

diode activation and current mismatch. Heavy shading reduces current further to 3.5 A, equating to a  $\sim$ 59% decrease compared with the unshaded condition, and the I–V curve becomes visibly compressed, reflecting restricted carrier flow and localized heating (Alombah et al., 2025). Panel (c) provides the time-synchronized correlation of tilt angle and shading index. While tilt oscillates gently between 28–32° (a range of only  $\pm$ 2°), the shading index varies sharply from 20% to 80%, showing that irradiance variability, not tilt fluctuations, primarily governs power degradation. The significant current reductions shown in panel (b) correspond directly to shading intensities captured in panel (c). These observations highlight that shading, even at modest levels, induces disproportionately large current and power losses, whereas tilt adjustments within a few degrees exert minimal influence. The combination of visual detection and electrical validation thus confirms the supervisory interface's capability to diagnose and quantify the real-time effects of shading on module performance.

#### **CONCLUSIONS**

The study showcased the creation and validation of a cutting-edge supervisory interface designed to enhance the performance evaluation of photovoltaic (PV) systems. This innovative tool seamlessly incorporates various PV setups, including isolated systems, grid-connected modules, fixed-tilt panels, and adjustable-tilt configurations. Such integration addresses the shortcomings found in traditional monitoring tools which often lack flexibility, real-time capabilities, and educational value. Through rigorous testing, the interface proved its ability to acquire real-time IV curves, monitor irradiance and temperature, and electronically control the inclination angles of the modules. One key finding was the identification of up to 50% power loss due to partial shading when just one cell of a 60-cell module was blocked, highlighting the system's sensitivity and efficiency over conventional methods. Additionally, a comparative analysis between merged and standalone systems revealed an 11% increase in energy output. Optimizing the angle settings resulted in a 14% improvement in irradiance capture when the tilt was adjusted from 0° to 34°. During peak sunlight, Module 2 maintained temperatures 3-5°C lower than Module 1, leading to better thermal efficiency. The measured temperature coefficients (-0.26%/°C) closely aligned with theoretical values (-0.24%/°C), validating the accuracy of the model. The study highlights the interface's utility in diagnosing system losses, testing various configurations, and enhancing energy harvesting in real-world conditions. As an educational tool, it encourages hands-on learning through remote and local experiments.

NEPT 27 of 31

However, the study also recommends further research to automate the mechanical tilt adjustment system, enhance resistance to environmental factors like wind loads, and improve software compatibility with other renewable energy platforms. Future studies could explore integrating predictive analytics and machine learning to forecast performance issues and optimize output dynamically. This work lays the groundwork for smart PV monitoring systems that can be adapted and scaled for global renewable energy applications.

#### **Conflict of Interest Statement:**

The author(s) declared no potential conflicts of interest.

## **Funding Declaration:**

No financial support was provided.

#### **Data Availability**

The datasets used during the current study are available from the corresponding author on reasonable request.

#### **REFERENCES**

- Alombah, N. H., Mungwe, J. N., Harrison, A., Fendzi Mbasso, W. F., & Fotsin, H. B. (2025). Advanced IoT-based monitoring system for real-time photovoltaic performance evaluation: Conception, development and experimental validation. *Scientific African*, 28. https://doi.org/10.1016/j.sciaf.2025.e02763
- Anand, A., A P Verayiah, R., Mansor, M., Tengku Hasim, T. J., Shukla, A., Panchal, H., Sharma, A., Natrayan, N., & Kumar, A. (2024). A comprehensive analysis of small-scale building integrated photovoltaic system for residential buildings: Techno-economic benefits and greenhouse gas mitigation potential. *Journal of Building Engineering*, 82. https://doi.org/10.1016/j.jobe.2023.108232
- Bhavani, N. G., Kumar, R., Panigrahi, B. S., Kishore, K., Arunsundar, B., Abdul-Samad, Z., & Singh, A. (2022). Design and implementation of iot integrated monitoring and control system of renewable energy in smart grid for sustainable computing network. *Sustainable Computing: Informatics and Systems*, 35. https://doi.org/10.1016/j.suscom.2022.100769
- Chung, J. Y., Park, M. H., Hong, S. H., Baek, J., Han, C., Lee, S., Kang, Y. T., & Kim, Y. (2023). Comparative performance evaluation of multi-objective optimized desiccant wheels coated with

NEPT 28 of 31

MIL-100 (Fe) and silica gel composite. *Energy*, 283. https://doi.org/10.1016/j.energy.2023.128567

- Daula Siddique, M., Prathap Reddy, B., Iqbal, A., Sarwar, A., Ahmed Memon, M., Dahri, K., & Mekhilef, S. (2022). A new design of active NPC converter topology with higher voltage gain for solar PV applications. *Sustainable Energy Technologies and Assessments*, 54. https://doi.org/10.1016/j.seta.2022.102850
- Dragicevic, T., Guerrero, J. M., Vasquez, J. C., & Skrlec, D. (2014). Supervisory control of an adaptive-droop regulated DC microgrid with battery management capability. *IEEE Transactions on Power Electronics*, 29(2), 695–706. https://doi.org/10.1109/TPEL.2013.2257857
- Ghaderi, D., Bayrak, G., & Guerrero, J. M. (2021). Grid code compatibility and real-time performance analysis of an efficient inverter topology for PV-based microgrid applications. *International Journal of Electrical Power and Energy Systems*, 128. https://doi.org/10.1016/j.ijepes.2020.106712
- Hamim Jeelani, S. H., Puviarasi, R., Chilambarasan, M., Shinde, S. S., Surakasi, R., Sharma, V., Singuru, S., Sudhakar, M., & Mohanavel, V. (2022). An approach to the utilization of grid integration to analyze the performance and quality of solar photovoltaic model. *Energy Reports*, 8, 1029–1044. https://doi.org/10.1016/j.egyr.2022.10.282
- He, W., Baig, M. J. A., & Iqbal, M. T. (2024). An Open-Source Supervisory Control and Data Acquisition Architecture for Photovoltaic System Monitoring Using ESP32, Banana Pi M4, and Node-RED. *Energies*, 17(10). https://doi.org/10.3390/en17102295
- Kalu, A., Emrich, C., Wilson, W., & Ventre, J. (1998). Photovoltaic-diesel hybrid supervisory control and data acquisition system design. *NASA Conference Publication*, 208413, 35.
- Khalid, W., Jamil, M., Khan, A. A., & Awais, Q. (2024). Open-Source Internet of Things-Based Supervisory Control and Data Acquisition System for Photovoltaic Monitoring and Control Using HTTP and TCP/IP Protocols. *Energies*, 17(16). https://doi.org/10.3390/en17164083
- Lv, X., Li, X., & Xu, C. (2023). A robust optimization model for capacity configuration of PV/battery/hydrogen system considering multiple uncertainties. *International Journal of Hydrogen Energy*, 48(21), 7533–7548. https://doi.org/10.1016/j.ijhydene.2022.11.220

NEPT 29 of 31

Maheri, A., Unsal, I., & Mahian, O. (2022). Multiobjective optimisation of hybrid wind-PV-battery-fuel cell-electrolyser-diesel systems: An integrated configuration-size formulation approach. *Energy*, 241. https://doi.org/10.1016/j.energy.2021.122825

- Mehmood, A., Saif, W., Habib, A., & Kalbani, A. (n.d.). Nature Environment and Pollution Technology An International Quarterly Scientific Journal Open Access Journal Original Research Paper Design and Impact Analysis of a Grid-Connected Solar Photovoltaic System in Ibri, Oman. 24, 1–18. https://doi.org/10.46488/NEPT.2024.v24iS1.001
- Patel, A., Gnana Swathika, O. V. G., Subramaniam, U., Thanikanti, T. S., Tripathi, A., Nag, S., Karthick, A., & Muhibbullah, M. (2022). A Practical Approach for Predicting Power in a Small-Scale Off-Grid Photovoltaic System using Machine Learning Algorithms. *International Journal of Photoenergy*, 2022. https://doi.org/10.1155/2022/9194537
- Pendem, S. R., & Mikkili, S. (2018). Modelling and performance assessment of PV array topologies under partial shading conditions to mitigate the mismatching power losses. *Solar Energy*, *160*, 303–321. https://doi.org/10.1016/j.solener.2017.12.010
- Rajamony, R. K., Kumar Pandey, A. K., Sofiah, A. G. N., Paw, J. K. S., Periyasami, G., Chopra, K., Subramaniyan, S., & Farade, R. A. (2024). Evaluating the energy and economic performance of hybrid photovoltaic thermal system integrated with multiwalled carbon nanotubes enhanced phase change material. *Materials Today Sustainability*, 28. https://doi.org/10.1016/j.mtsust.2024.101035
- Ramesh, S., Manikandan, T., Rajaram, R., Arul, U., Michael, G., & Selvakumar, A. (2023). Vehicular network energy storage system with renewable analysis using deep learning architectures. *Computers and Electrical Engineering*, 110. https://doi.org/10.1016/j.compeleceng.2023.108801
- Rinesh, S., Arun, M., Kumar, S. N., Prajitha, C., & Senthil Kumar, A. P. S. (2025). Evaluating the type 2 fuzzy logic controller with multilayer perceptrons for optimal tracking of solar photovoltaic systems. *International Journal of Low-Carbon Technologies*, 20, 394–403. https://doi.org/10.1093/ijlct/ctaf016
- Robalo, B. M. B., & Figueiredo, J. M. G. (2010). Supervisory control developed for a solar tracking prototype based on PV-technology. *IFAC Proceedings Volumes (IFAC-PapersOnline)*, 1(PART 1), 291–296. https://doi.org/10.3182/20100329-3-pt-3006.00053

NEPT 30 of 31

Scravaglieri, L., Popov, M., Lima Pilla, L., Guermouche, A., Aumage, O., & Saillard, E. (2023). Optimizing performance and energy across problem sizes through a search space exploration and machine learning. *Journal of Parallel and Distributed Computing*, 180, 104720. https://doi.org/10.1016/j.jpdc.2023.104720

- Sudhahar, S., Shanmugasundaram, R., Kumar, R. J., & Ashok, B. (2025). An interleaved converter topology and optimized controller for electric vehicle drive utilizing solar photovoltaic system. *Electrical Engineering*, 107(2), 1719–1743. https://doi.org/10.1007/s00202-024-02584-5
- Vargas-Salgado, C., Aguila-Leon, J., Chiñas-Palacios, C., & Hurtado-Perez, E. (2019). Low-cost web-based Supervisory Control and Data Acquisition system for a microgrid testbed: A case study in design and implementation for academic and research applications. *Heliyon*, 5(9). https://doi.org/10.1016/j.heliyon.2019.e02474
- Veríssimo, P. H. A., Campos, R. A., Guarnieri, M. V., Veríssimo, J. P. A., do Nascimento, L. R., & Rüther, R. (2020). Area and LCOE considerations in utility-scale, single-axis tracking PV power plant topology optimization. *Solar Energy*, 211, 433–445. https://doi.org/10.1016/j.solener.2020.09.070
- Xia, X., Liu, Z., Wang, Z., Sun, T., & Zhang, H. (2023). Multi-layer performance optimization based on operation parameter-working fluid-heat source for the ORC-VCR system. *Energy*, 272. https://doi.org/10.1016/j.energy.2023.127103
- Xiao, W., Torchyan, K., El Moursi, M. S., & Kirtley, J. L. (2014). Online supervisory voltage control for grid interface of utility-level PV plants. *IEEE Transactions on Sustainable Energy*, *5*(3), 843–853. https://doi.org/10.1109/TSTE.2014.2306572
- Xie, A., An, L., Chen, H., Xue, X., & Xu, G. (2023). Performance optimization of the air-cooling system in a coal-fired power unit based on intelligent algorithms. *Applied Thermal Engineering*, *230*. https://doi.org/10.1016/j.applthermaleng.2023.120791
- Xu, L., Yang, Z., Xi, L., Duan, D., Yang, X., Gao, J., & Li, Y. (2023). Multi-objective performance optimization of target surface of bionic blue whale-skin impinged by array jet. *International Communications in Heat and Mass Transfer*, 141. https://doi.org/10.1016/j.icheatmasstransfer.2022.106611

NEPT 31 of 31

Zhang, X., Zhang, X., Ma, M., Sun, Y., & Ma, C. (2023). Rapid performance optimization strategy of MK-FA-GBFS based geopolymer foam heavy-metal adsorbent. *Construction and Building Materials*, 394. https://doi.org/10.1016/j.conbuildmat.2023.132161

- Zhu, Z., Sun, S., & Huang, S. (2025a). ILADRC resonance suppression control strategy for multiple parallel photovoltaic energy storage GFL VSG microgrid. *Electrical Engineering*, 107(3), 3591–3604. https://doi.org/10.1007/s00202-024-02706-z
- Zhu, Z., Sun, S., & Huang, S. (2025b). ILADRC resonance suppression control strategy for multiple parallel photovoltaic energy storage GFL VSG microgrid. *Electrical Engineering*, 107(3), 3591–3604. https://doi.org/10.1007/s00202-024-02706-z